JOURNAL OF AIRCRAFT
Vol. 40, No. 2, March–April 2003

Fuselage Shape Optimization of a Wing–Body Configuration with Nacelles

Yoshikazu Makino* and Toshiyuki Iwamiya†
National Aerospace Laboratory, Tokyo 182-8522, Japan
and
Zhong Lei‡
VINAS Company, Ltd., Osaka 550-0002, Japan

An aerodynamic design tool that combines a computational fluid dynamics code with an optimization technique for a drag minimization is developed and applied to a fuselage shape optimization of a Mach 1.7 scaled supersonic experimental airplane. An airframe/nacelle integration is taken into consideration. The optimized fuselage is compared with a conventional axisymmetrical area-ruled fuselage designed by a linear theory. The results indicate that a nonaxisymmetrical fuselage design concept with this optimization design tool is effective for the reduction of pressure drag, especially in the design of an airplane that generates a strong interference drag between its airframe and nacelles.

Nomenclature

C_{Dp}	=	pressure drag coefficient
C_L	=	lift coefficient
C_p	=	pressure coefficient
H	=	Heaviside step function
I	=	object function in optimization process
K	=	penalty function coefficient in optimization process
L	=	airplane length
M	=	Mach number
R	=	fuselage radius
V	=	fuselage volume
x	=	axial coordinate of airplane
α	=	angle of attack
Δs	=	computational grid spacing
μ	=	Mach angle

Subscripts

min	=	minimum value
0	=	initial value

Introduction

AIRPLANE drag reduction is important in the design of an economically feasible next-generation supersonic transport (SST). One drag count ($C_D = 0.0001$) reduction of an SST airplane reduces airplane gross weight by 4700 kg and saves 3400 kg of fuel. This is equivalent to reduction in the structural weight of more than 1 ton (Ref. 1). The National Aerospace Laboratory (NAL) of Japan started a scaled supersonic experimental airplane program, National Experimental Supersonic Transport (NEXST)[2] in 1996 to establish advanced technologies, including a computational fluid dynamics (CFD)-based design tool for the drag reduction of the SST. In this program, flight tests of an uncrewed nonpowered experimental airplane (NEXST-1) will be conducted. This airplane was designed for Mach 2.0 using NAL's original aerodynamic design technology together with CFD prediction. Its design features for high lift/drag ratio include a cranked arrow wing, a modulated warp, an area-ruled configuration, and a natural laminar flow wing. The engine installation influences both wave drag due to volume and the drag due to lift. Many theoretical and experimental studies for the reduction of an airframe/nacelle interference drag are conducted.[3–5] The authors developed a CFD-based total aerodynamic design tool[6] for the design of a jet-powered experimental airplane (NEXST-2) to reduce the airframe/nacelle interference drag. This aerodynamic design tool combines a CFD code with an optimization technique. A three-dimensional Euler CFD code[6] with an overset-grids technique[7] is used for solving the flowfield around a complex airplane configuration. An advantage of the overset-grids technique for a CFD-based aerodynamic design is the ease of regenerating computational grids for shape modifications because a computational grid is generated independently around each airplane component. For the optimization process, a quasi-Newton optimization technique based on a conjugate gradient method[8] is adopted. The flow chart of this design tool is shown in Fig. 1. One design cycle of the quasi-Newton optimization method has two steps: a gradient calculation of the object function and a line minimization in the direction that is a conjugate to the calculated steepest direction. In the gradient calculation, the design tool utilizes an adjoint sensitivity analysis.[9,10] The computational cost for the sensitivity analysis of the optimization process is largely reduced by the adjoint method, compared with a finite difference gradient calculation. The adjoint method used in this design tool has been validated by comparing the adjoint gradients and finite difference gradients of the object function with respect to all design variables. The design tool has been applied to several test cases of the drag minimization problem, such as a simple axisymmetrical body and two bodies under a wing–body configuration.[6] The main objective of this research is to find an effective design concept for the reduction of an airframe/nacelle interference drag by applying the design tool to a fuselage shape optimization of the jet-powered experimental airplane.

In the next section, the SST configuration optimized in this paper, and its computational grid used in the CFD analyses, are described. Results obtained applying the design tool to a fuselage shape optimization of a wing–body configuration and a wing–body configuration with two flow-through nacelles are then presented. Two types of design spaces, an axisymmetrical and a nonaxisymmetrical fuselage

Received 2 May 2001; presented as Paper 2001-2447 at the AIAA 19th Applied Aerodynamics Conference, Anaheim, CA, 11 June 2001; revision received 20 July 2002; accepted for publication 18 September 2002.

*Researcher, Next Generation Supersonic Transport Project Center, 7-44-1 Jindaijihigashi, Chofu. Member AIAA.
†Director, Computational Fluid Dynamics Technology Center, 7-44-1 Jindaijihigashi, Chofu. Member AIAA.
‡Computational Fluid Dynamics Engineer, 1-18-35 Edobori, Nishi.

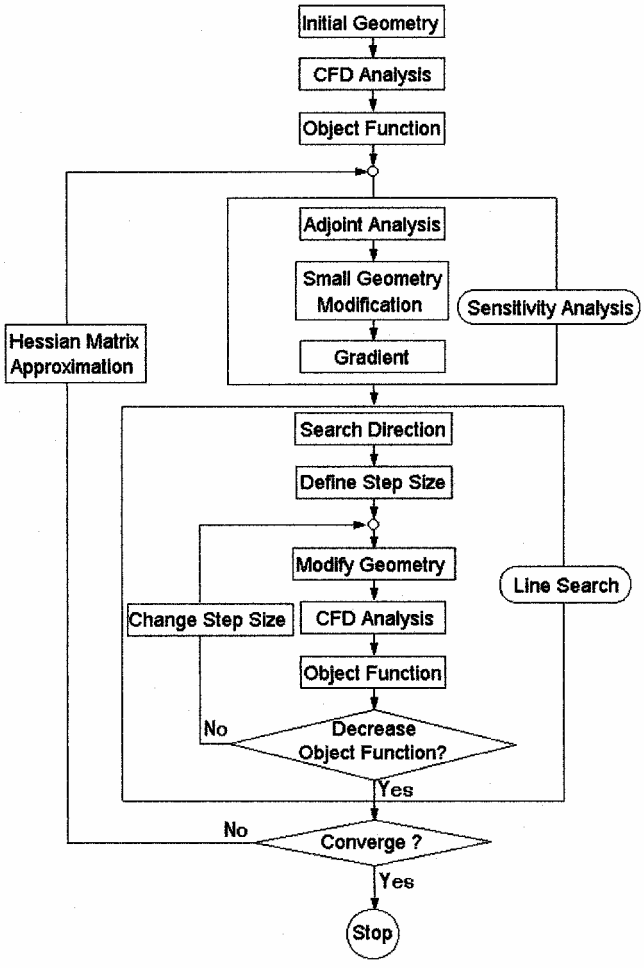

Fig. 1 Shape optimization flow chart.

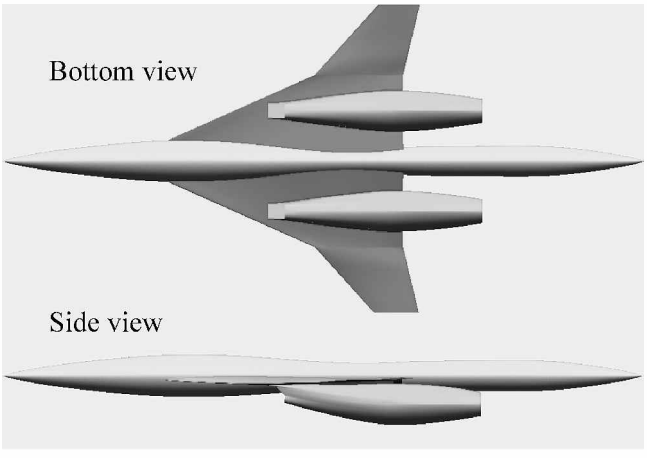

Fig. 2 Wing–Body configuration with nacelles.

shape modification, are used in the case of the wing–body configuration with two flow-through nacelles.

SST Configuration

The SST configuration, whose fuselage shape is optimized in this paper, is shown in Fig. 2. This configuration is one of the candidates of the jet-powered experimental airplane in its conceptual design phase. Its design Mach number is $M = 1.7$. Its length is 10.057 m, wing area is 10.12 m^2, and the wing aspect ratio is 2.4. The nacelle length is 3.37 m, which is rather large for the scaled airplane. This is because we use existing jet engines for the jet-powered experimental airplane, whereas the airplane configuration itself is scaled for

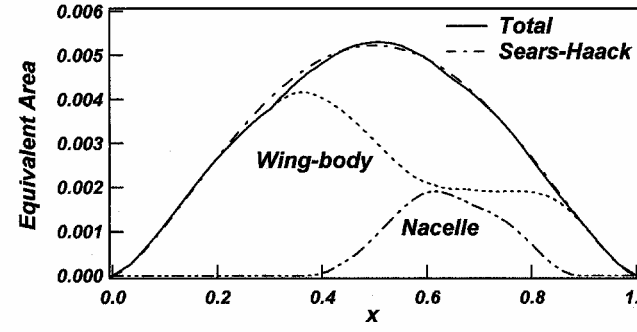

Fig. 3 Equivalent area distribution of the area-ruled airplane.

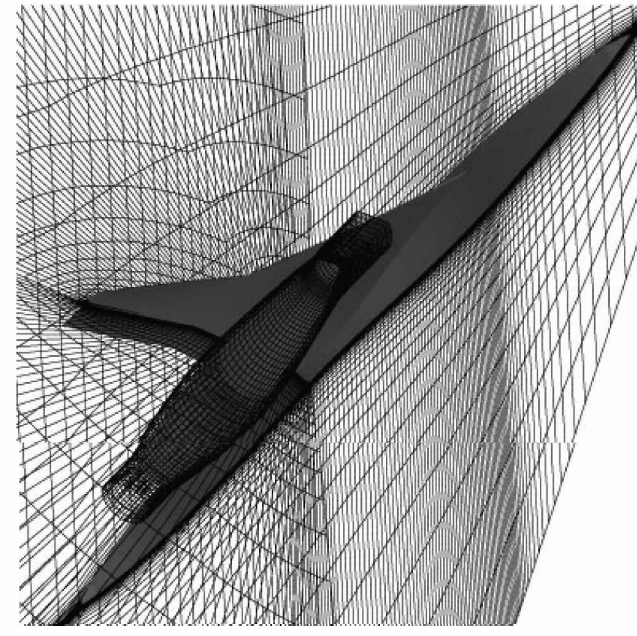

Fig. 4 Computational grids.

the flight tests. The optimized fuselage geometry obtained in the design process is compared with an axisymmetrical area-ruled fuselage that is designed using a CAD system so that the total equivalent area distribution of the aircraft is equal to that of a Sears–Haack body. Figure 3 shows the total equivalent area distribution of the configuration shown in Fig. 2, compared with the target area distribution of the Sears–Haack body. In this study, a total equivalent area distribution of a wing–body configuration with nacelles is determined as follows:

1) Define a cutting plane at a given point on the airplane axis whose normal vector is inclined at the angle of $\pi/2 - \mu$ from the axis.

2) Generate a cross section of each airplane component intercepted by the cutting plane.

3) Define an equivalent area as a summation of the frontal projection areas of all cross sections.

4) Rotate the cutting plane at the angle of $2\pi/N$ around the airplane axis and calculate the equivalent area in the same way as 2 and 3.

5) Repeat stage 4 N times and average all N equivalent areas.

6) Repeat stages 1–5 from the nose to the tail of the airplane.

$N = 24$ is used in this study. Figure 4 shows the computational grids around the configuration used in the CFD analyses. A major grid is generated around the wing–body configuration and a minor grid is generated around the nacelle. The minimum grid spacing on the body surface of these grids are $\Delta s_{\min}/L = 0.0001$. The major grid is regenerated for every CFD calculation for the fuselage shape modification to avoid grid skewness and the change of minimum grid spacing that are accompanied by the modification of the former

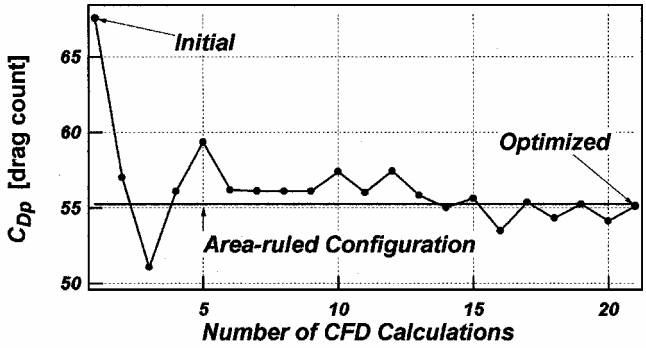

a) History of pressure drag coefficient

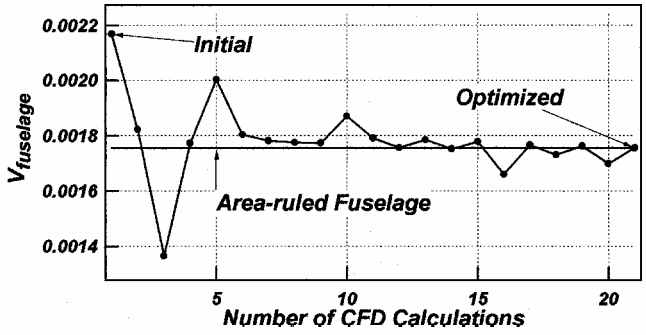

b) History of fuselage volume

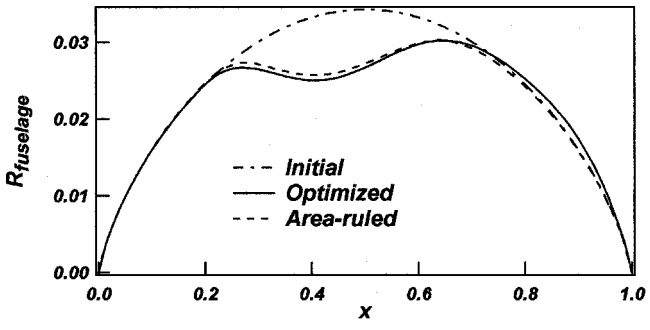

c) Optimized fuselage geometry

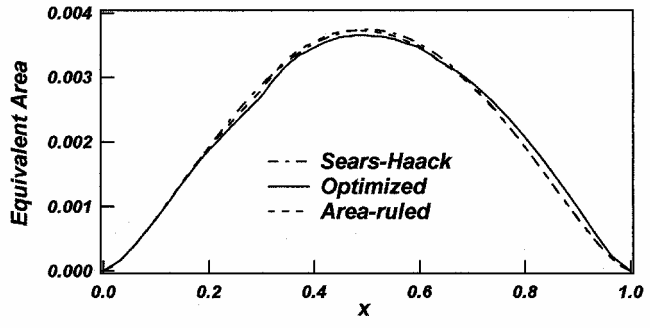

d) Equivalent area distributions

Fig. 5 Fuselage shape optimization result without nacelles.

grid. The CFD code is validated by comparing its computational results of a similar SST configuration with the experimental data.[6]

Design Results

In this section, the design tool is applied to a fuselage shape optimization of wing–body configurations with and without nacelles.

Wing–Body Without Nacelles

In the optimization process of a wing–body configuration without nacelles, the object function to be minimized is

$$I = \left\{C_{Dp} + K[(V - V_{\min})/V_{\min}]^2 H(V_{\min} - V)\right\} \Big/ C_{Dp0} \qquad (1)$$

where C_{Dp} is for a wing–body configuration that is obtained by the CFD analysis. The second term of the numerator is the penalty function that keeps the fuselage volume no less than a specified minimum value $V_{\min}$, which is the area-ruled fuselage volume in the design. The function $H(y)$ is the Heaviside step function, which has a value of 1 when y has a positive value and 0 when y is less than 0. K influences the convergence rate of the design. In this study, it is set to 50, which is determined not to hinder the convergence from some design tests. An initial fuselage geometry is the Sears–Haack body, whose area distribution is used as a target distribution for the area-ruled wing–body configuration. The initial fuselage geometry is modified axisymmetrically by adding radial changes whose axial distribution is defined by a 12th-order Bezier curve controlled by 13 points, including two fixed points at the fuselage nose and tail. The radial coordinates of the other 11 points are used as design variables in the optimization process. The optimization result is shown in Fig. 5. Figures 5a and 5b show the convergence histories of the pressure drag coefficient and fuselage volume with respect to the number of CFD calculations. After 21 CFD calculations (nine design cycles), the pressure drag coefficient is reduced about 18% from the initial configuration, and both the pressure drag coefficient and fuselage volume are at about the same level as those of the area-ruled configuration. The fuselage geometry and total equivalent area distribution of the optimized configuration shown in Figs. 5c and 5d, respectively, are about the same as those of the area-ruled configuration.

Wing–Body with Nacelles

Next, the design tool is applied to the wing–body configuration with two nacelles shown in Fig. 2. The object function is the same as Eq. (1), where C_{Dp} represents the pressure drag coefficient of the wing–body configuration and the outer surfaces of two flow-through nacelles in this case. Three types of Bezier curves controlled by three sets of design variables are checked before the shape optimization. In these checks, each curve is added to the initial Sears–Haack body to minimize the following object function:

$$I = \int |R_{\text{target}} - R| \, \mathrm{d}x \qquad (2)$$

where the target radius distribution R_{target} is the original area-ruled fuselage. As shown in Fig. 6, the fuselage represented by a 16th-order Bezier curve is quite similar to the area-ruled fuselage, whereas the 8th- and 12th-order Bezier curves are different from the area-ruled fuselage. Therefore, a 16th-order Bezier curve is used for a shape modification in the following cases.

Axisymmetrical Fuselage Modification

At first, the fuselage geometry is modified axisymmetrically by a 16th-order Bezier curve. There are 15 design variables. Figure 7 shows the fuselage shape optimization result. The pressure drag coefficient is reduced about 22% from the initial configuration after 19 CFD calculations (eight design cycles), and both the pressure drag coefficient and fuselage volume are at about the same level as those of the area-ruled configuration. The optimized fuselage geometry and total equivalent area distribution, however, are different from those of the area-ruled configuration. The pressure drag coefficient of each airplane component is shown in Table 1. The pressure drag coefficient of the inner duct surfaces of two flow-through nacelles of the optimized configuration, which is not included in the object function, is about the same as that of the area-ruled configuration. Although the total pressure drag coefficient of the optimized configuration is about the same as that of the area-ruled configuration, the drag of the wing–body configuration is decreased 2.6 drag counts and that of two nacelle outer surfaces is increased 2.2 drag counts. This result suggests that the area-ruled axisymmetrical fuselage, based on a linear theory using a CAD system, is not

Table 1 Pressure drag coefficient of each airplane component

Fuselage	α, deg	Wing–Body, $C_{Dp} \times 10^4$	Nacelles (outer) $C_{Dp} \times 10^4$	Nacelles (inner) $C_{Dp} \times 10^4$	Total $C_{Dp} \times 10^4$	Lift C_L
Area-ruled	0.0	60.9	125.6	−15.2	171.3	0.027
Optimized (axisymmetrical)	0.0	58.3	127.8	−15.1	171.0	0.027
Optimized (nonaxisymmetrical)	0.0	59.1	121.5	−15.3	165.3	0.021
Optimized (nonaxisymmetrical)	0.19	57.3	123.1	−15.2	165.2	0.028

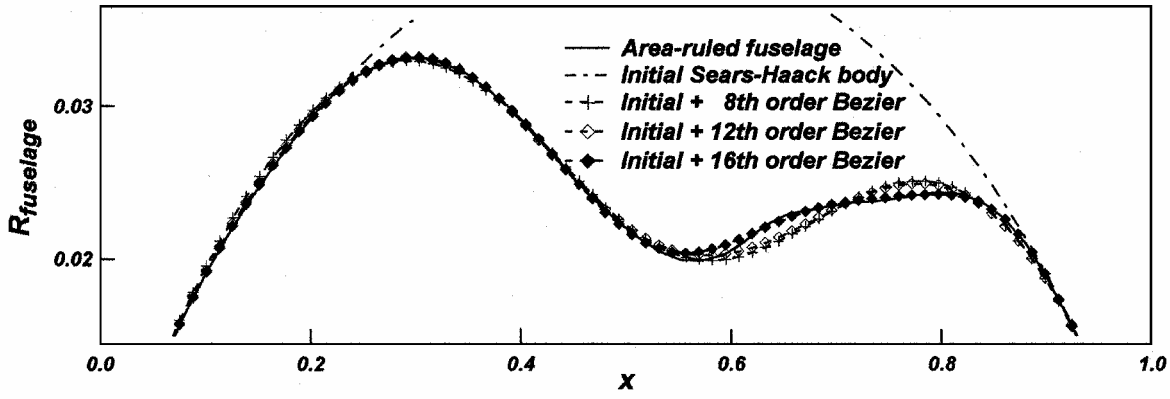

Fig. 6 Difference between shape modification methods.

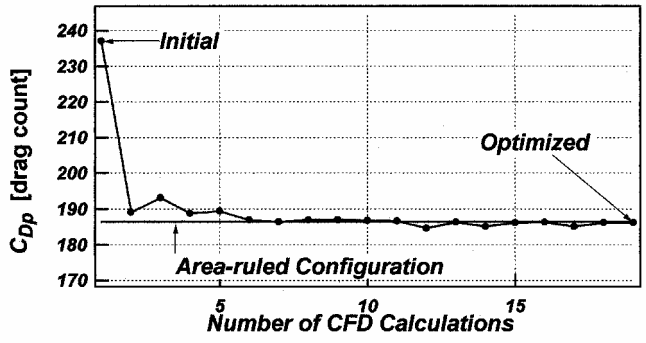

a) History of pressure drag coefficient

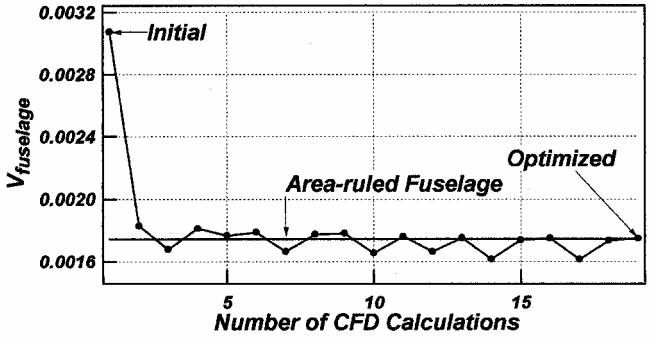

b) History of fuselage volume

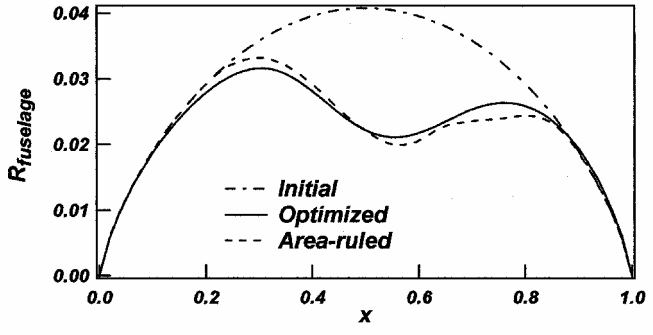

c) Optimized fuselage geometry

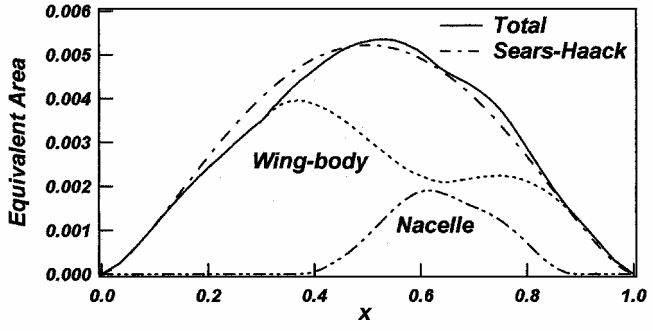

d) Equivalent area distributions

Fig. 7 Axisymmetrical fuselage shape optimization result with nacelles.

a unique solution of a minimum pressure drag configuration if an airplane generates a strong interference drag between its airframe and nacelles. In this case, the optimization design tool found another solution in the design space starting from the initial Sears–Haack body. The original area-ruled fuselage can be found by the design tool if another initial configuration is selected. The total lift coefficient (C_L) of the airplane is also shown in Table 1. Although a fixed lift coefficient constraint is not given in this shape optimization, the lift coefficient does not change during the design process in the case of the axisymmetrical fuselage modification.

Nonaxisymmetrical Fuselage Modification

Next, the design space is extended to a nonaxisymmetrical fuselage whose upper, lower, and side radius distributions on the airplane axis are modified separately from the initial geometry. Each radius modification method is the same as the axisymmetrical fuselage case; therefore, the total number of design variables used in this case are $15 \times 3 = 45$. The axisymmetrical area-ruled fuselage represented by a 16th-order Bezier curve, shown in Fig. 6, is used as an initial geometry. As shown in Figs. 8a and 8b, the pressure drag coefficient of the optimized configuration is about 3% smaller than that of the area-ruled configuration, whereas their fuselage volumes are about the same. Figure 8c shows top and side views of the optimized fuselage compared with the initial geometry. The lower fuselage shape becomes different from the upper and side shape and shows a rapid decrease of the radius at $x = 0.3$–0.5. It seems that the increase of the equivalent area at about $x = 0.4$ for the nacelles shown in Fig. 8d is canceled by only the lower part of the fuselage.

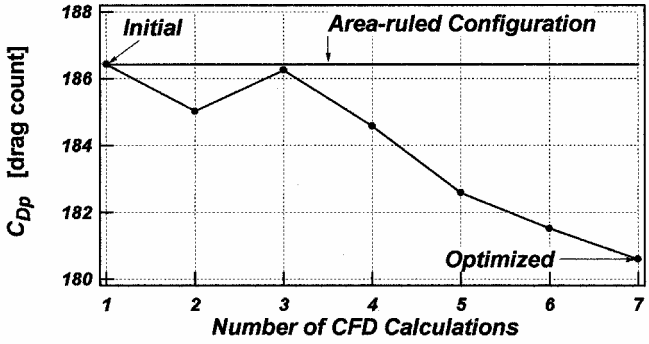

a) History of pressure drag coefficient

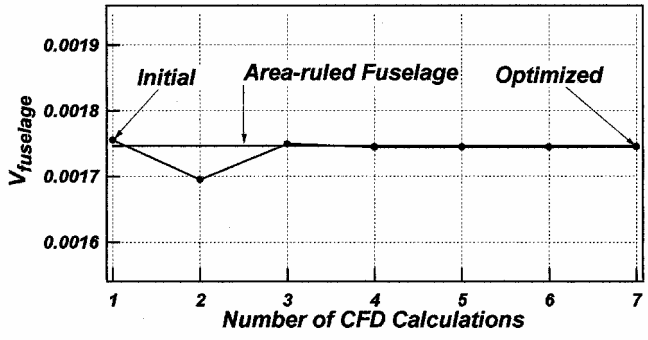

b) History of fuselage volume

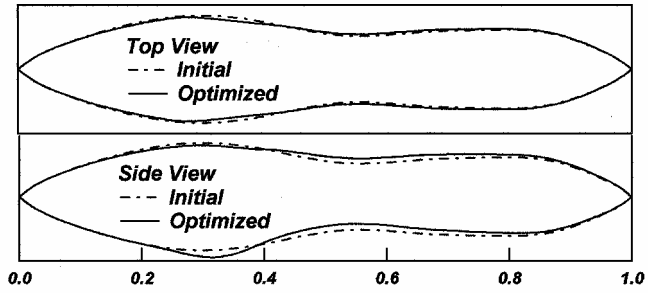

c) Optimized fuselage geometry

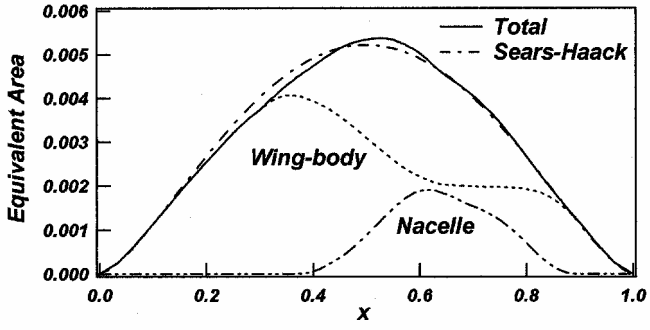

d) Equivalent area distributions

Fig. 8 Nonaxisymmetrical fuselage shape optimization result with nacelles.

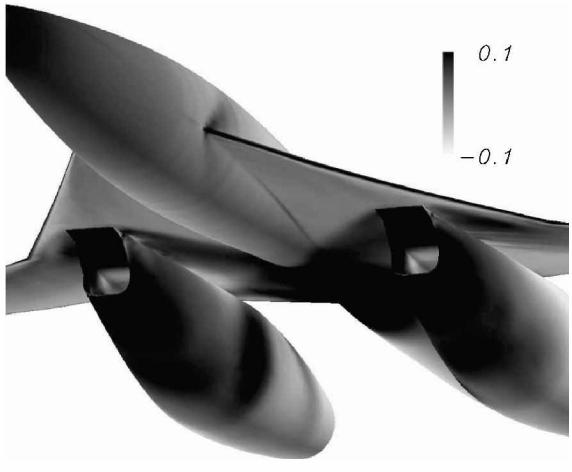

a) Initial area-ruled configuration

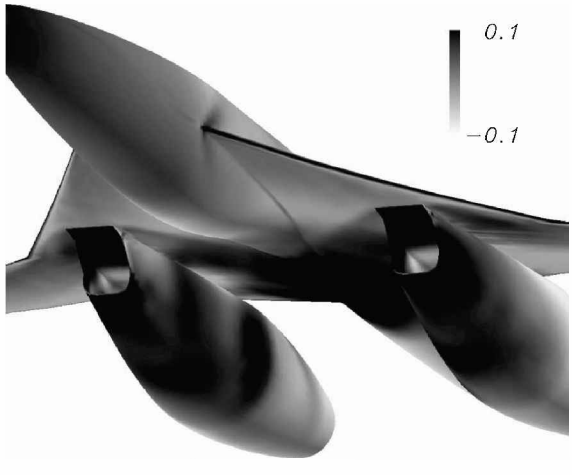

b) Optimized configuration with a nonaxisymmetrical fuselage

Fig. 9 Iso-C_p contours on airplane surfaces.

As shown in Table 1, the total pressure drag coefficient is reduced 6.0 drag counts, in which 1.8 drag counts are due to the wing–body and 4.1 drag counts are due to two nacelle outer surfaces. The main reduction of the pressure drag is due to the nacelle outer surfaces. Figures 9a and 9b show the C_p contours of the initial and optimized airplane surfaces, respectively. It is seen that the strong expansion generated from the optimized fuselage interferes with the shocks from the nacelle intakes and reduces the pressure on the nacelle outer surfaces. Although the optimized fuselage geometry is considerably different from the area-ruled fuselage, the total equivalent area distribution of the optimized configuration shown in Fig. 8d is not so different from that of the Sears–Haack body compared with the axisymmetrical fuselage case shown in Fig. 7d. This suggests that the optimized fuselage may be one of the candidates that satisfy the area rule in the nonaxisymmetrical fuselage design space. The design tool selected the geometry that minimized the interference drag between the wing–body and nacelles.

The lift coefficient of the optimized configuration ($C_L = 0.021$) shown in Table 1 is smaller than that of the area-ruled one ($C_L = 0.027$) because the expansion generated from the fuselage reduces the pressure on the wing lower surface. Therefore, the pressure drag coefficient of the optimized configuration is recalculated by the Euler CFD code at the angle of attack $\alpha = 0.19$ deg and shown in Table 1. The result shows that the total pressure drag coefficient of the optimized configuration is still smaller than that of the area-ruled one at the same lift coefficient.

Conclusions

Fuselage shape optimizations of wing–body configurations with and without nacelles are conducted by an aerodynamic design tool that combines a three-dimensional Euler CFD code with a gradient-based optimization technique. The fuselage geometry obtained in the optimization process of the wing–body configuration without nacelles is about the same as the area-ruled fuselage. An axisymmetrical and a nonaxisymmetrical fuselage shape modification are used in the case of the wing–body configuration with two flow-through nacelles. The axisymmetrical optimized fuselage geometry is different from the axisymmetrical area-ruled fuselage, whereas the pressure drag coefficient and fuselage volume of the optimized configuration are about the same as those of the area-ruled configuration. This suggests that the area-ruled fuselage is not a unique

solution of a minimum pressure drag configuration if an airplane generates a strong interference drag between its airframe and nacelles. The design tool found the optimized configuration with a nonaxisymmetrical fuselage, whose total pressure drag coefficient is smaller than that of the area-ruled configuration. Infinite airplane configurations that satisfy the area-rule can exist in a nonaxisymmetrical fuselage design space, and the optimized airplane configuration seems to be one of them. The result indicates that this aerodynamic design tool has the ability to select a better configuration among many area-ruled configurations, taking into consideration the interference drag between an airframe and nacelles.

Acknowledgments

The authors are grateful to Ken'ichiro Suzuki for his cooperation in the calculation of the equivalent area by CAD and to Fumitake Kuroda for his cooperation with the grid generation.

References

[1]Kulfan, B. M., "Reynolds Numbers Considerations for Supersonic Flight," AIAA Paper 2002-2038, June 2002.

[2]Sakata, K., "Supersonic Experimental Airplane Program in NAL (NEXST) and its CFD-Design Research Demand," International Workshop on Numerical Simulation Technology for Design of Next Generation Supersonic Civil Transport, SP-49T, NAL, Chofu, Tokyo, Japan, 2000, pp. 53–56

[3]Sigalla, A., and Hallstaff, T. H., "Aerodynamics of Powerplant Installation on Supersonic Aircraft," *Journal of Aircraft*, Vol. 4, No. 4, 1967, pp. 273–277.

[4]Benson, J. L., Sedgwick, T. A., and Wright, B. R., "Supersonic Cruise Vehicle Propulsion System Integration Studies," AIAA Paper 76-756, July 1976.

[5]Welge, H. R., Radkey, R. L., and Henne, P. A., "Nacelle Aerodynamic Design and Integration Study on a Mach 2.2 Supersonic Cruise Aircraft," AIAA Paper 76-757, July 1976.

[6]Makino, Y., and Iwamiya, T., "Numerical Simulation and Aerodynamic Design of an SST Configuration with Nacelles," AIAA Paper 2000-0126, Jan. 2000.

[7]Benek, J. A., Buning, P. G., and Steger, J. L., "A 3-D Chimera Grid Embedding Technique," AIAA Paper 85-1523, July 1985.

[8]Press, W. H., Teukoisky, S. A., Vetterling, W. T., and Flannery, B. P., *Numerical Recipes in FORTRAN*, 2nd ed., Cambridge Univ. Press, Cambridge, England, U.K., 1992, pp. 418–423.

[9]Jameson, A., "Optimum Aerodynamic Design Using CFD and Control Theory," *12th AIAA Computational Fluid Dynamics Conference*, AIAA Paper 95-1729-CP, AIAA, Washington, DC, 1995, pp. 926–949.

[10]Reuther, J., "Aerodynamic Shape Optimization Using Control Theory," Ph.D. Dissertation, Dept. of Mechanical and Aeronautics, Univ. of California, Davis, CA, June, 1996.